

## Morphological Effects of Alkylated Multiwalled Carbon Nanotubes on Poly(L-lactic acid)-Based Composites

Young Soo Yun, Ha Il Kwon, Hyeonseong Bak, Eun Ju Lee, Jin-San Yoon, and Hyoung-Joon Jin\*

Department of Polymer Science and Engineering, Inha University, Incheon 402-751, Korea

Received February 1, 2010; Revised April 27, 2010; Accepted April 30, 2010

**Abstract:** This study examined the reinforcing effects of multiwalled carbon nanotubes (MWCNTs) with different morphologies in a poly(L-lactic acid) (PLLA) matrix. The surfaces of the MWCNTs were modified using linear alkyl chains to disperse the MWCNTs homogeneously in the polymer matrix. The morphology of the MWCNTs was determined from numerical values for the  $D_b$ ,  $l_{sp}$  and  $I_G/I_D$ . These numerical values were related to the morphology of the MWCNTs and had an effect on the PLLA/MWCNT composites. The rod-like MWCNTs with a relatively high  $D_b$ ,  $l_{sp}$  and  $I_G/I_D$  exhibited superior electrical and thermal properties owing to their morphological characteristics, such as their more crystallized  $sp^2$  carbon structure, high contour length and static bending persistence. Therefore, rod-like MWCNTs are more advantageous than those with a bent morphology with respect to MWCNT reinforced polymer composite applications.

**Keywords:** multiwalled carbon nanotubes, morphology, poly(L-lactic acid), nanocomposite.

### Introduction

Carbon nanotubes (CNTs) have drawn a great deal of attention because of their novel potential as polymer additives and fillers.<sup>1-3</sup> Many efforts have been made to develop CNT-reinforced composite materials, such as epoxy resins,<sup>4,5</sup> thermoplastics<sup>6-9</sup> and natural polymers.<sup>3,10</sup> However, aside from the reinforcing effects of CNTs with different surface functionalities on a polymer matrix, research related to the reinforcing effects of CNTs with different morphologies is insufficient. Theoretically, CNTs that are made of a rolled graphene layer or layers should be straight in shape. However, the heptagon-pentagon pair and others pairs, which are generated in the CNT synthesis process, permanently bend the tube. Therefore, CNTs have various morphologies with respect to their bending degree.<sup>11</sup> These CNTs with various morphologies can be characterized using quantitative factors such as the bending ratio ( $D_b$ ), the mean square end-to-end distance ( $\langle R^2 \rangle$ ), and the square contour length ( $L^2$ ).<sup>12</sup>

$$D_b = \frac{\langle R^2 \rangle}{L^2} \quad (1)$$

$$\langle R^2 \rangle = 2l_{sp}L + 2l_{sp}^2(e^{-L/l_{sp}} - 1) \quad (2)$$

The modulus of the polymer-multiwalled carbon nanotube (MWCNT) composites depends on the degree of curvature of the MWCNTs. Additionally, the electrical properties of the polymer-MWCNTs depend on the contour length or the static bending persistence length ( $l_{sp}$ ).<sup>12</sup>

The nano-size and the high aspect ratio of the CNTs enable the electrical percolation at a very low loading, which enhances the electrical conductivity even at a very low additive concentration. The presence of the CNTs also improves the mechanical properties compared to the conventional composites containing carbon black.<sup>4-6</sup> A homogeneous dispersion of the CNTs in the polymer matrix is crucial to the electrical and mechanical properties in order to maximize the reinforcing effects of the CNTs. A high dispersity of CNTs results in low percolation thresholds and superb reinforcing effects.<sup>5,14</sup>

Presently, poly(L-lactic acid) (PLLA) is one of the most attractive and promising candidates as a replacement for petrochemical products because it is not only biodegradable but is also produced from renewable natural resources through the fermentation of polysaccharide or sugar, e.g., from corn and beets. Therefore, the biological cycle comes full circle with the PLLA biodegradation and the photosynthesis processes.<sup>15,16</sup> Additionally, the high mechanical performance and the low production cost of PLLA make it applicable as a packaging material for a broader array of products.<sup>17</sup>

In this study, the reinforcing effects of the MWCNTs with two types of morphologies (rod-like and bent MWCNTs) were investigated in the PLLA matrix. The surface of the MWCNTs was modified using a linear alkyl chain in order

\*Corresponding Author. E-mail: hjin@inha.ac.kr

to create a homogeneous MWCNT dispersion in the PLLA matrix. At low MWCNT concentrations, all of the alkylated MWCNT (MWCNT-C<sub>12</sub>) incorporated composites exhibited enhanced mechanical and thermal properties, as well as electrical percolation thresholds. The rod like MWCNTs (r-MWCNTs) exhibited better electrical properties than the bent MWCNTs (b-MWCNTs) in the PLLA/MWCNT composite. Therefore, the anti-static function was induced using a small quantity of the r-MWCNTs in the PLLA/MWCNT composite.

## Experimental

**Preparation of Surface Modified MWCNTs.** The as-received r-MWCNTs (NCT, Japan) and b-MWCNTs (Iljin Nanotech, Korea) were treated with acid using the following procedure, which was reported in an earlier study.<sup>10</sup> The MWCNTs were treated in an acid mixture (sulfuric acid/nitric acid=3:1 (v/v)) at 60 °C (r-MWCNT-COOH and b-MWCNT-COOH) in order to remove any impurities within the MWCNTs through the introduction of carboxylic and hydroxyl functional groups onto the surface of the MWCNTs. Then the alkylated MWCNTs were prepared using a linear alkyl chain.<sup>18</sup> The alkylated MWCNTs exhibited a good dispersity and stability in organic solvents. The nomenclatures for the rod-like and bent alkylated MWCNTs were r-MWCNT-C<sub>12</sub> and b-MWCNT-C<sub>12</sub>, respectively.

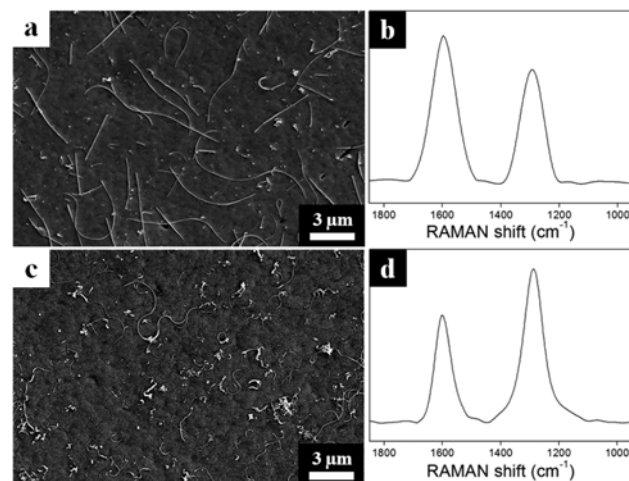
**Preparation of PLLA/MWCNT Composite.** A certain amount of the MWCNT-C<sub>12</sub> was dispersed into chloroform through ultrasonication for 1 h. Then 3.0 g of PLLA was dissolved in the MWCNT dispersion with continuous stirring. The mixture was cast in a glass dish and dried for 48 h at room temperature. All of the tensile dumb-bell bars were made using a Mini max molder at 180 °C. The hot mold was allowed to naturally cool at ambient temperature. The dumb-bell specimens were made according to the ASTM D 638 standard for tensile testing.

**Characterization.** The morphologies of the MWCNTs and the MWCNT incorporated composites were observed using field emission scanning electron microscopy (FESEM, S-4300SE, Hitachi, Japan) at an accelerating voltage of 15 kV after the samples were pre-coated with a homogeneous Pt layer through ion sputtering (E-1030, Hitachi, Japan). Raman spectroscopy (BRUKER RFS-100/S, 1064 nm excitation, Germany) was used to determine the presence of sp<sup>2</sup> hybridized carbon by examining the E<sub>2g</sub> mode or the G band (stretching vibrations in the basal plane of the crystalline graphite), the so-called D band (indicating the level of the defects in the graphitic material), and the I<sub>G</sub>/I<sub>D</sub> ratio (D band to G band intensity ratio, which is normally used to assess the purity and the crystallinity) of the MWCNT samples. The electrical conductivities of the MWCNT and the porous MWCNT electrodes were measured using a four-probe method with an electrical conductivity meter (Hiresta-UP

MCP-HT450, Mitsubishi Chemical, Japan). Differential scanning calorimetry (DSC) was carried out using a Perkin-Elmer 7 instrument, with dry nitrogen gas at a flow rate of 20 mL/min. The DSC was calibrated using indium as the standard, and the sample weight was maintained at 7.0 ± 0.1 mg. The thermal history of the products was removed by scanning them from 30 to 190 °C at a heating rate of 20 °C/min. The thermal stability was estimated using thermogravimetric analysis (TGA, TA instruments, Q50, UK) at a heating rate of 20 °C/min from room temperature to 800 °C in air. The tensile properties were tested on an Instron 4665 ultimate tensile testing machine (UTM) at 20 °C and a humidity of 30%. The cross-head speed was set at 10 mm/min for both of the dumb-bell samples. At least 5 specimens of a given sample were collected and averaged for the tensile property tests. The quantitative analysis of the atomic content of the modified clays was identified through elemental analysis (EA) (Censtruments Thermo EA111,2 England).

## Results and Discussion

The morphologies of the r-MWCNTs and the b-MWCNTs are depicted in Figure 1. The r-MWCNTs exhibited a straight line morphology with a relatively high I<sub>G</sub>/I<sub>D</sub> ratio of 1.38. In contrast, the b-MWCNTs had a winding morphology with a relatively low I<sub>G</sub>/I<sub>D</sub> ratio of 0.71. According to equations (1) and (2), the r-MWCNTs had a D<sub>b</sub> of 0.85, a contour length of 4,747 nm, and a l<sub>sp</sub> of 4,500 nm. On the other hand, the b-MWCNTs had a D<sub>b</sub> of 0.43, a contour length of 565 nm, and a l<sub>sp</sub> of 184 nm. These factors provided numerical information about the morphologies of the MWCNTs. The r-MWCNTs exhibited relatively high values for the D<sub>b</sub>, l<sub>sp</sub> and I<sub>G</sub>/I<sub>D</sub> ratio, suggesting that the main-frame consisted of a relatively large amount of crystalline sp<sup>2</sup> hybridized carbon. The degree of functionalization was

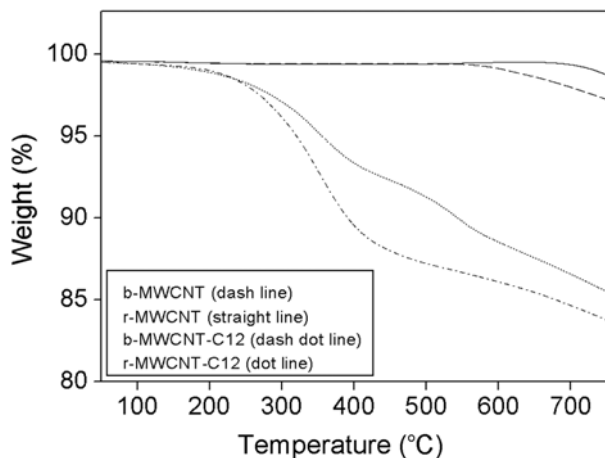
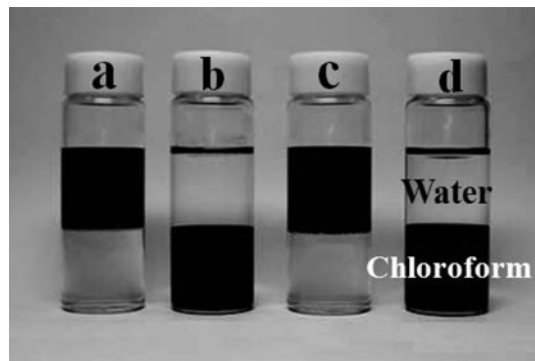


**Figure 1.** SEM images and Raman spectra of the MWCNTs: (a), (b) r-MWCNTs and (c), (d) b-MWCNTs.

**Table I. Elementary Analysis (EA) of the Pristine, Acid Treated, and Alkylated MWCNTs**

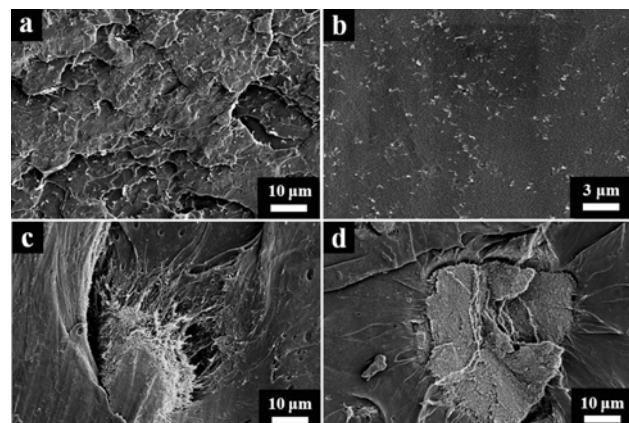
Sample Name	C (wt%)	O (wt%)	H (wt%)
b-MWCNT	99.01	0	0.09
r-MWCNT	99.04	0	0.06
b-MWCNT-COOH	87.25	12.20	0.55
r-MWCNT-COOH	92.5	8.31	0.44
b-MWCNT-C <sub>12</sub>	92.08	5.47	1.45
r-MWCNT-C <sub>12</sub>	95.16	4.11	0.73

characterized using the EA and TGA data. Table I shows the EA data of the pristine, acid treated and alkylated MWCNTs. All of the pristine MWCNTs consisted of only carbon except for a small amount of hydrogen. After the pristine MWCNTs were acid treated, the oxygen content of the b-MWCNTs and the r-MWCNTs increased by 12.20 and 8.31 wt%, respectively, because of the surface functionalization that was caused by the carboxylic acid and hydroxyl groups on the surface of the MWCNTs. The oxygen content of b-MWCNT-COOH was larger than r-MWCNT-COOH. Therefore, the oxidization ratio of b-MWCNTs with a relatively large amount of defect sites was higher than the r-MWCNTs because the defect sites of the MWCNTs were easily attacked by the acid. For the alkylated MWCNTs, the carbon and hydrogen contents of both r-MWCNT-C<sub>12</sub> and b-MWCNT-C<sub>12</sub> increased, which suggested that the alkylated MWCNTs were successfully synthesized. Figure 2 shows the TGA data of the pristine and alkylated MWCNTs. The b-MWCNTs decomposed at about 550 °C, whereas the r-MWCNTs decomposed at about 680 °C because of the different defect ratios for the two MWCNTs. The TGA curves of the alkylated MWCNTs exhibited an obvious weight loss at 250 °C, which was attributed to the loss of the alkyl chains. The weight loss between 250 and 430 °C was used

**Figure 2.** TGA data for the pristine and alkylated MWCNTs.**Figure 3.** Dispersion of the (a) r-MWCNT-COOH, (b) r-MWCNT-C<sub>12</sub>, (c) b-MWCNT-COOH, and (d) b-MWCNT-C<sub>12</sub> composites in a water/chloroform solution.

to estimate the weight percentage of the alkyl chains that were attached to the tubes, which was 10 and 6 wt% for b-MWCNT-C<sub>12</sub> and r-MWCNT-C<sub>12</sub>, respectively.

Figure 3 shows the dispersion of various types of MWCNTs. All of the MWCNT-C<sub>12</sub>s were homogeneously dispersed in chloroform because of the physical repulsion and the chemical hydrophobic properties of the linear alkyl chains. These hydrophobic properties also led to a homogeneous dispersion in the PLLA matrix. Figure 4 shows the SEM images of the fracture surfaces of the PLLA/MWCNT-C<sub>12</sub> and PLLA/MWCNT-COOH composites. The MWCNT-COOHs were aggregated in the PLLA matrix, and micrometer-scale agglomerations sporadically formed. In contrast, both the r-MWCNT-C<sub>12</sub> and the b-MWCNT-C<sub>12</sub> were homogeneously dispersed in the PLLA matrix, increasing the interfacial adhesion between the MWCNTs and the PLLA matrix, which resulted in low percolation thresholds and superb reinforcing effects. Therefore, the surface modification pro-

**Figure 4.** SEM images of the fracture surfaces of the PLLA/MWCNT-C<sub>12</sub> and PLLA/MWCNT-COOH composites: (a) r-MWCNT-C<sub>12</sub>, (b) b-MWCNT-C<sub>12</sub>, (c) r-MWCNT-COOH, and (d) b-MWCNT-COOH incorporated composites.

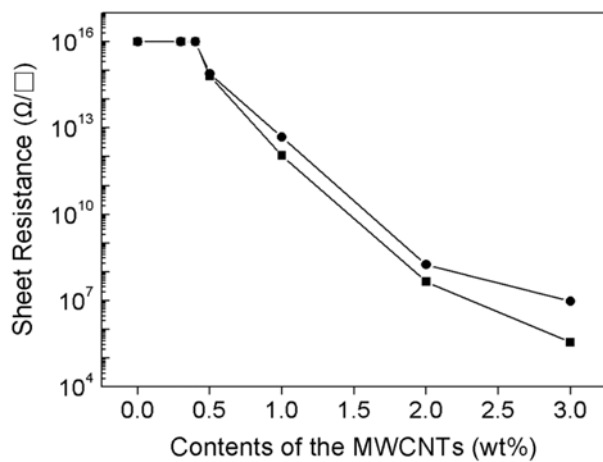


**Figure 5.** Surface resistivity of the PLLA/r-MWCNT-C<sub>12</sub> (square) and PLLA/b-MWCNT-C<sub>12</sub> (circle) composites at various MWCNT contents.

cess with a hydrophobic material was required in order to investigate the reinforcing effects of the nano-sized MWCNTs. The physical properties of the composite were maximized through this process. These PLLA/MWCNT-C<sub>12</sub> composites exhibited electrical percolation thresholds at low MWCNT-C<sub>12</sub> contents below 0.5 wt% (Figure 5). When 3 wt% of the MWCNTs were introduced into the PLLA matrix, the sheet resistances of the r-MWCNT and b-MWCNT incorporated composites greatly increased over 11 orders of magnitude to values of  $3.6 \times 10^5 \Omega/\square$  and  $9.5 \times 10^6 \Omega/\square$ , respectively, corresponding to electrostatic dissipative plastics. The r-MWCNT-C<sub>12</sub> incorporated composite exhibited a lower sheet resistance than the b-MWCNT-C<sub>12</sub> incorporated composite because of its more crystallized sp<sup>2</sup> carbon structure as well as its high contour length and static bending persistence length ( $l_{sp}$ ). The mechanical and thermal properties of the PLLA matrix were determined in order to investigate the reinforcing effects of the r-MWCNT-C<sub>12</sub> and the b-MWCNT-C<sub>12</sub> by introducing 0.5 wt% of the MWCNT-C<sub>12</sub>, which was around the electrical percolation threshold. Figure 6 shows the DSC thermograms of the 1st cooling and 2nd heating for the PLLA/MWCNT-C<sub>12</sub> composites. The re-crystallization temperatures of the PLLA/r-MWCNT-C<sub>12</sub> and PLLA/b-MWCNT-C<sub>12</sub> were higher than the pristine PLLA. Additionally, the full widths of the melting and crystallization peaks at half maximum were narrower than the pure PLLA. Therefore, the crystallite size distribution was narrower in

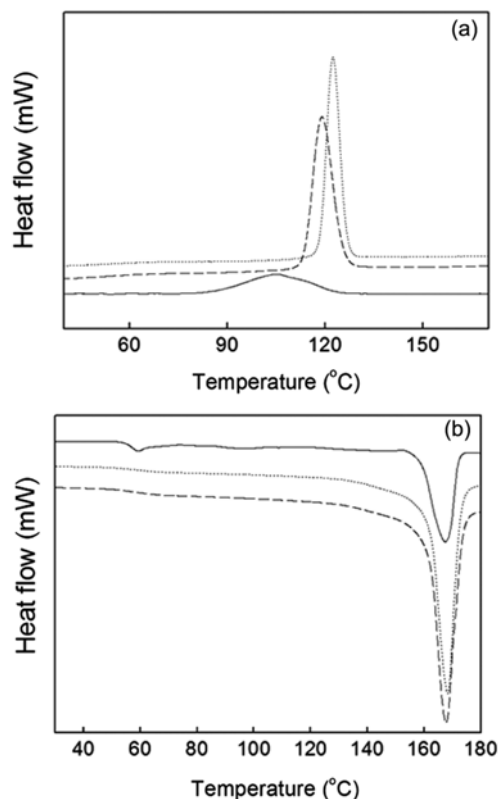


**Figure 6.** DSC thermograms of pure PLLA (solid) and the PLLA/r-MWCNT-C<sub>12</sub> (dot) and PLLA/b-MWCNT-C<sub>12</sub> (dash) composites at a content of 0.5 wt%: (a) 1st cooling and (b) 2nd heating.

the PLLA/MWCNT-C<sub>12</sub> composites than the pure PLLA. Compared to the polymer, the higher thermal conductivity of the MWCNTs was responsible for the sharper crystallization and melting peaks because the heat was more evenly distributed in the samples containing the MWCNTs. The r-MWCNTs exhibited a better thermal conductivity because of their morphological characteristics.<sup>19</sup> Therefore, the crystallization and melting peaks were sharper compared to the b-MWCNT-C<sub>12</sub> incorporated composite. Table II shows the thermal properties of the PLLA/MWCNT-C<sub>12</sub> composites. The positive effects of the thermal properties were induced by introducing the MWCNTs into the PLLA matrix. The r-MWCNT-C<sub>12</sub> induced a slightly high thermal degradation temperature ( $T_d$ ) for the composite compared to the b-MWCNT-C<sub>12</sub> because of the relatively high thermal conduc-

**Table II. Thermal Properties of Pure PLLA and the PLLA/MWCNT-C<sub>12</sub> Composites at a Content of 0.5 wt%**

Sample Name	$T_m$ (°C)	$T_c$ (°C)	$\Delta H_m$ (J/g)	$\Delta H_c$ (J/g)	$T_d$ (°C)
PLLA	167.5	104.9	-37.25	38.52	302.0
PLLA/r-MWCNT-C <sub>12</sub>	168.3	122.4	-41.31	41.56	309.8
PLLA/b-MWCNT-C <sub>12</sub>	167.7	119.0	-38.18	40.58	308.9

**Table III. Mechanical Properties of Pure PLLA and the PLLA/MWCNT-C<sub>12</sub> Composites at a Content of 0.5 wt%**

Sample Name	Tensile Stress (MPa)	Young's Modulus (GPa)	Elongation at Break (%)
PLLA	53.1 ± 2.3	1.2 ± 0.1	13.5 ± 0.6
PLLA/r-MWCNT-C <sub>12</sub>	58.0 ± 2.8	1.4 ± 0.1	14.5 ± 0.9
PLLA/b-MWCNT-C <sub>12</sub>	59.8 ± 2.2	1.6 ± 0.2	13.5 ± 0.7

tivity of the r-MWCNT-C<sub>12</sub>. Table III shows the mechanical properties of the PLLA/MWCNT-C<sub>12</sub> composites. The tensile strength and modulus of the PLLA/MWCNT-C<sub>12</sub> composites improved after the introduction of the MWCNT-C<sub>12</sub>s. The length and the aspect ratio of the MWCNTs that reinforced the polymer were critical to both the load transfer efficiency and the effective modulus of the composites. The MWCNTs with a long length and a high aspect ratio exhibited improved mechanical properties.<sup>20,21</sup> However, no enormous differences were observed between the r-MWCNT-C<sub>12</sub> and b-MWCNT-C<sub>12</sub> incorporated composites. Contrary to the predicted results, the tensile strength and the Young's modulus of the b-MWCNT-C<sub>12</sub> incorporated composite were slightly high because of the degree of alkylation, not the difference in the shape of the MWCNTs. The interfacial adhesion between the b-MWCNTs and the PLLA matrix was better than the r-MWCNTs because the b-MWCNTs contained 10 wt% of alkyl chains. However, more research related to the morphologies of the MWCNTs and their mechanical properties is still required.

Based on these results, the fundamental differences between the rod-like and the bent-like MWCNTs were considered in the PLLA/MWCNT composites. The factors that impacted the morphological effects of the alkylated MWCNTs in the PLLA/MWCNT composites were their shape and degree of defects. The rod-like shape was more advantageous in the percolation of the electrical or thermal conduction

compared to the bent-like shape. Additionally, the defects in the MWCNTs had an adverse effect on the overall properties of the PLLA/MWCNT composites. The number of defects in the MWCNTs decreased as the shape of the MWCNTs became more rod-like. Figure 7 shows the Raman data and the SEM images of various MWCNTs. The degree of defects in the MWCNTs was determined from the  $I_G/I_D$  ratio using Raman spectroscopy. The MWCNTs with a relatively large amount of defects had a more winding morphology. These results suggested that the morphology and the defects of the MWCNTs were interdependent. Therefore, one part of the morphological effects of the MWCNT was caused by the inherent defects of the MWCNTs in PLLA/MWCNT composites.

## Conclusions

The reinforcing effects of the alkylated MWCNTs with two types of morphologies (rod-like and bent MWCNTs) were investigated in the PLLA matrix. The r-MWCNTs had a  $D_b$  of 0.85, a contour length of 4747 nm, a  $l_{sp}$  of 4,500 nm, and an  $I_G/I_D$  of 1.38, whereas the b-MWCNTs had a  $D_b$  of 0.43, a contour length of 565 nm, a  $l_{sp}$  of 184 nm, and an  $I_G/I_D$  of 0.71. These numerical values were related to the morphologies of the MWCNTs and had an effect on the PLLA/MWCNT composites. The morphological effects of the MWCNTs were caused by both the shape and the defects of the MWCNTs in the PLLA/MWCNT composites. The shape of the MWCNTs had an effect on the percolations of the electrical or thermal conductivity. Additionally, the defects in the MWCNTs had an adverse effect on the overall properties of the PLLA/MWCNT composites. The two types of MWCNT-C<sub>12</sub> incorporated composites exhibited electrical percolation thresholds and enhanced thermal and mechanical properties at low MWCNT contents. However, the r-MWCNT-C<sub>12</sub> incorporated composites exhibited superior electrical and thermal properties because of their advantageous morphological characteristics, such as a more crystallized  $sp^2$  carbon structure as well as a high contour length and static bending persistence. Therefore, the anti-static function was more effectively induced using small quantities of the r-MWCNT-C<sub>12</sub> in the PLLA/MWCNT composites.

**Acknowledgements.** This work was financially supported by a grant from the Fundamental R&D Program for Core

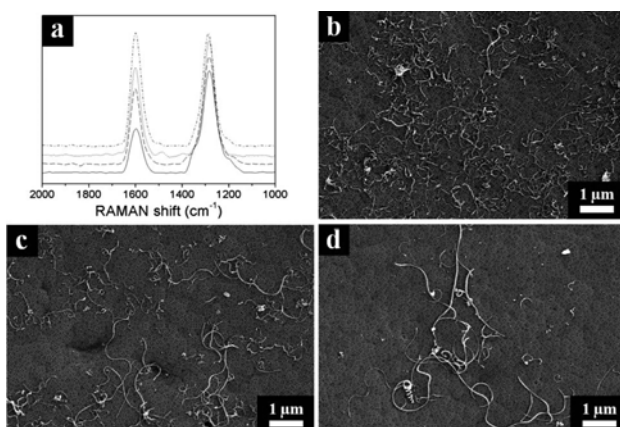


**Figure 7.** (a) Raman spectra of various MWCNTs with different  $I_G/I_D$  ratios (straight line: 0.44, dash line: 0.71, dot line: 0.76 and dash dot line: 1.00) and SEM images of various MWCNTs with different  $I_G/I_D$  ratios ((b) 0.44, (c) 0.71, and (d) 0.76).

Technology of Materials funded by the Ministry of knowledge Economy, Republic of Korea.

## References

- (1) D. Tasis, N. Tagmatarchis, A. Bianco, and M. Prato, *Chem. Rev.*, **106**, 1105 (2006).
- (2) M. Kang, S. J. Myung, and H.-J. Jin, *Polymer*, **47**, 3961 (2006).
- (3) S. H. Yoon, H.-J. Jin, M.-C. Kook, and Y. R. Pyun, *Biomacromolecules*, **7**, 1280 (2006).
- (4) C. A. Martin, J. K. W. Sandler, M. S. P. Shaffer, M.-K. Schwarz, W. Bauhofer, K. Schulte, and A. H. Windle, *Compos. Sci. Technol.*, **64**, 2309 (2004).
- (5) J. K. W. Sandler, J. E. Kirk, I. A. Kinloch, M. S. P. Shaffer, and A. H. Windle, *Polymer*, **44**, 5893 (2003).
- (6) S. B. Kharchenko, J. F. Douglas, J. Obrzut, E. A. Grulke, and K. B. Migler, *Nature Mater.*, **3**, 564 (2004).
- (7) O. Meincke, D. Kaempfer, H. Weickmann, C. Friedrich, M. Vathauer, and H. Warth, *Polymer*, **45**, 739 (2004).
- (8) P. Pötschke, T. D. Fornes, and D. R. Paul, *Polymer*, **43**, 3247 (2002).
- (9) O. Regev, P. N. B. Elkati, J. Loos, and C. E. Koning, *Adv. Mater.*, **16**, 248 (2004).
- (10) S.-M. Kwon, H.-S. Kim, and H.-J. Jin, *Polymer*, **50**, 2786 (2009).
- (11) H. S. Lee, C. H. Yun, H. M. Kim, and C. J. Lee, *J. Phys. Chem. C*, **111**, 18882 (2007).
- (12) H. S. Lee, C. H. Yun, S. K. Kim, J. H. Choi, C. J. Lee, H.-J. Jin, H. Lee, S. J. Park, and M. Park, *Appl. Phys. Lett.*, **95**, 134104 (2009).
- (13) F. T. Fisher, R. D. Bradshaw, and L. C. Brinson, *Compos. Sci. Technol.*, **63**, 1689 (2003).
- (14) Y. F. Shih, L. S. Chen, and R. J. Jeng, *Polymer*, **49**, 4602 (2008).
- (15) R. E. Drumright, P. R. Gruber, and D. E. Henton, *Adv. Mater.*, **12**, 1841 (2000).
- (16) A. Södergård and M. Stolt, *Prog. Polym. Sci.*, **27**, 1123 (2002).
- (17) R. Auras, B. Harte, and S. Selke, *Macromol. Biosci.*, **4**, 835 (2004).
- (18) Y. Kim, S.-M. Kwon, D.-Y. Kim, H.-S. Kim, and H.-J. Jin, *Curr. Appl. Phys.*, **9**, 100 (2009).
- (19) P. C. Song, C. H. Liu, and S. S. Fan, *Appl. Phys. Lett.*, **88**, 153111 (2006).
- (20) H. Wan, F. Delale, and L. Shen, *Mech. Res. Commun.*, **32**, 481 (2005).
- (21) K. K. H. Wong, M. Zinke-Allmang, J. L. Hutter, S. Hrapovic, J. H. T. Luong, and W. Wan, *Carbon*, **47**, 2571 (2009).